CHAPTER-Four

Chapter four deals with the polyethylenimine mediated synthesis and characterization of nanocrystalline PBNPs. As synthesized Prussian blue nanoparticles was further self assembled to the gold nanoparticles and used for electrocatalytic detection of hydrogen peroxide sensing. Peroxidase like mimetic activity was analyzed for both PBNPs and gold nanoparticles assembled Prussian blue nanoparticles.

Polyethylenimine mediated Synthesis of Prussian blue nanoparticles and cooperative self assembly of gold nanoparticles on Polycationic surface

1 Polyethylenimine mediated synthesis of Prussian blue nanoparticles and cooperative self assembly of gold nanoparticles on Polycationic surface

1.1 Introduction

The structural, electronic and magnetic properties of Prussian blue (PB) studied in the past decade revealed that the Prussian blue and its analogues behave as high-temperature molecular magnets, photo-switchable magnetic solids, antidotes for radioactive poisoning, molecular sieves, electrocatalytic and hydrogen storage materials [(Ding *et al.* 2009; Entley and Girolami 1995; Ferlay *et al.* 1995; Holmes and Girolami 1999; Kaye and Long 2005; Sato *et al.* 1996; Shatruk *et al.* 2007)]. The variety of promising properties notwithstanding, it is an ongoing challenge to establish an accurate composition of PB, given an inherent structural disorder [(Samain *et al.* 2013)], a situation which necessitates the controlled synthesis of Prussian blue. Further, all Prussian blues are highly insoluble [(Samain *et al.* 2013)], with a solubility product of ca. 1×10^{-41}, the preparation of water soluble PB is of fundamental and technological interests since they may be easier to manipulate and thus to integrate into future molecule-based electronic devices. Accordingly, attempts have been made to control Prussian blue nucleation preventing extended network as stabilized Prussian blue nanoparticles (PBNPs) [(Pandey and Pandey 2013c)]. The earlier findings demonstrated that the use of 3-aminopropyltrimethoxysilane (3-APTMS) along with cyclohexanone allow controlled conversion of processable PBNPs from single precursor potassium ferricyanide [$K_3Fe(CN)_6$] with the average particle size to the order of 15.6 nm justifying impressive electron transfer rate constant [32.1 s^{-1}] [(Pandey and Pandey 2013c)]. Similar method was used for the controlled synthesis of mixed metal analogues having super peroxidase mimetic activity [(Pandey and Pandey 2013d)]. However, the use of 3-APTMS during operation and processing of PBNPs introduced additional problems associated to auto hydrolysis, condensation and poly condensation of alkoxy-group thereby reducing the practical usability of nanomaterial in specific concern and

directed for suitable substitute of 3-APTMS. Fortunately, we succeeded to replace 3-APTMS by tetrahydrofuran-hydroperoxide (THF-HP) which efficiently enabled the conversion of $K_3[Fe(CN)_6]$ into water soluble PBNPs under ambient condition [(Pandey and Pandey 2014a)]. The use of THF-HP again directed us to evaluate the contribution of tetrahydrofuran (THF) and hydrogen peroxide (H_2O_2) during the synthesis of PBNPs [(Pandey and Panday 2016b)]. It was found that $K_3[Fe(CN)_6]$ undergo controlled conversion into water soluble PBNPs in the presence of THF and H_2O_2 at 60 °C within 3 hours justifying both homogeneous and heterogeneous catalysis [(Pandey and Panday 2016b)]. The PBNPs made through the participation of 3-APTMS and cyclohexanone [(Pandey and Pandey 2013d)] yielded polycrystalline PBNPs whereas the use of THF-HP [(Pandey and Pandey 2014a)] and THF along with H_2O_2 [(Pandey and Panday 2016b)] resulted decrease in polycrystalline behaviour of the same. The decrease in polycrystalline behaviour of Prussian blue may be followed by slower electrocatalytic activity in many concern and directed to manifest the polycrystalline behaviour through suitable reaction protocol for controlled conversion of single precursors $K_3[Fe(CN)_6]$ into PBNPs.

Prussian blue made from double precursors leads to the formation of crystalline Prussian blue with limited solubility. Recently, the role of polyethylenimine (PEI) has been demonstrated that allowed the conversion of double precursors into Prussian blue Nanocubes [(Zhai *et al.* 2008)]. PEI-Protected Prussian Blue Nanocubes with edge length of 50 nm and uniform size was made from double precursor in acidic medium containing PEI, $FeCl_3$, $K_3[Fe(CN)_6]$ and KCl [(Zhai *et al.* 2008)]. Since, the use of double precursor introduces non-processability for electroanalytical applications, we intended to synthesize water soluble PBNPs involving the contribution of PEI from single precursor $K_3[Fe(CN)_6]$. Indeed, excellent finding on the synthesis of polycrystalline PBNPs having superparamagnetic behaviour has been recorded. As made PBNPs are processable having potentiality for the fabrication of PBNPs-modified electrode justifying excellent

electrochemical activity for both electrochemical oxidation and reduction of H_2O_2. In addition to that as made PBNPs also displays homogeneous catalysis as peroxidase mimetics. The catalytic activity of Prussian blue can further be manipulated through incorporating AuNPs [(Jing *et al.* 2014; Qiu *et al.* 2007)]. The synthesis of PB@Au was carried out from the use of double precursors and the gold cations were reduced from the use of trisodium citrate and tannic acid [(Jing *et al.* 2014; Qiu *et al.* 2007)]. The use of PEI for the conversion of $K_3[Fe(CN)_6]$ in to PBNPs along with reduction of gold cations is desirable. The use of PEI has been demonstrated for the reduction of gold cations into AuNPs through thermal process [(Mohammed *et al.* 2013; Sun *et al.* 2004, 2006; Wen *et al.* 2013)]. Further, we have recently demonstrated the role of PEI for controlled conversion of gold cations into gold nanoparticles (AuNPs) [(Pandey *et al.* 2016)]. Accordingly, attempt the use of PEI may allow the as an efficient reagent both making PBNPs-AuNPs composite and indeed interesting finding on self assembly of AuNPs on surface of cationic polymer protected PBNPs is recorded. The data recorded on as made nanomaterials based on UV-Vis spectroscopy, TEM, XRD, cyclic voltammetry and magnetic measurements are reported in this chapter.

1.2 Experimental

1.2.1 Material and Methods

Potassium ferricyanide $K_3[Fe(CN)_6]$ and hydrogen peroxide (H_2O_2) were purchased from Merck, India. Polyethylenimine (PEI) (mol wt 60,000), nujol oil (density 0.838 gml^{-1}), graphite powder (particle size 1-2 μm), and o-dianisidine were purchased from Sigma- Aldrich Chemical Co., India. Tetrachloroauric acid ($HAuCl_4$) was purchased from HiMedia, India. All aqueous solutions were prepared by using double distilled-deionised water (Alga water purification system). All Chemicals used were of analytical grade. All the experiments were performed at room temperature unless otherwise mentioned.

1.2.2 Synthesis of cationic polymer coated nanocrystalline PBNPs and AuNPs assembled PBNPs

Typical process of PBNPs synthesis involves the mixing of 70 µl aqueous solution of $K_3[Fe(CN)_6]$ (0.05 M) and 20 µl of PEI (0.1 g/ml) under stirred condition over a vertex cyclomixer followed by addition of 5 µl hydrochloric acid (HCl) (6.5 M). The resultant mixture was kept at 60 °C in an oven for 3 hours. The yellow colour solution turned in to deep blue colour which indicates the formation of PBNPs as evaluated from the absorption maxima recorded at 680 nm. The optimum concentrations of $K_3[Fe(CN)_6]$ and PEI were achieved by varying the concentrations of one component while keeping fixed concentrations of other and *vice versa* as composition shown in Table.4.1. and Table.4.2.

Table.4.1. Characteristics of PBNPs as a function of PEI concentration.

Vial	$K_3[Fe(CN)_6]$ (mol L^{-1})	PEI (mg/ml)	PBNPs sol formation	Extent of Formation
A	0.025	10	Light Blue	-
B	0.025	20	Dark Blue	+++
C	0.025	30	Light Blue	++
D	0.025	40	Greenish Blue	+

Table.4.2. Characteristics of PBNPs as a function of $K_3[Fe(CN)_6]$ concentration.

Vial	$K_3[Fe(CN)_6]$ (mol L^{-1})	PEI (mg/ml)	PBNPs sol formation	Extent of Formation
A	0.010	20	Light Blue	+
B	0.025	20	Dark Blue	++
C	0.035	20	Dark Blue	+++
D	0.050	20	Light Blue	+

Synthesis of self assembly of AuNPs on polycationic surface PBNPs was conducted by allowing PEI mediated AuNPs formation in Prussian blue solution. Typically, 100 µl of PEI coated PBNPs were mixed with 40 µl of $HAuCl_4$ (25 mM) and kept at 60 °C for 5 minutes in an incubator oven.

1.2.3 Measurement and characterization

All UV-Vis spectroscopy experiments were performed by using Hitachi U-2900 spectrophotometer.

X-ray diffraction (XRD) patterns were collected at a Rigaku miniflex II diffractometer using CuKα (λ= 1.506Å) radiation. A continuous mode was used for data collection in the 2θ range from 10° to 90° at a scanning speed of 4° min^{-1}. The crystallite size was calculated as described in chapter-2. XRD analysis was performed on the powder sample which was obtained by drying the PBNPs solution at 60 °C overnight in a vacuum oven.

To know the particles size, Transmission Electron Microscopy (TEM) analysis was performed. TEM analysis of as synthesized PBNPs and AuNPs assembled PBNPs was done with a JEOL JEM-2100F electron microscope operated at 200 kV. Sample preparation for the TEM analysis, a drop of the PBNPs or AuNPs assembled PBNPs solution was drop casted

onto carbon coated copper grid (Mesh size-400) obtained from M/s. Electron Microscopy Sciences, USA. Drop casted carbon coated copper grid was dried at room temperature and used for TEM analysis.

The magnetic properties of the PB samples were measured on a Magnetic Property Measurement System (MPMS®3) (Quantum Design Inc., MPMS-XL, USA). MPMS measurement was performed on the powder sample which was obtained as described in XRD analysis.

The electrochemical measurements were performed with electrochemical workstation CHI 660B (CH instrument, USA).

1.2.4 Electrochemical measurements and preparation of modified graphite paste electrode

The electrochemical measurements were done on CHI 660B Electrochemical workstation in a three electrodes configuration with a working solution of 3 ml. The working electrode was PBNPs or AuNPs assembled PBNPs modified graphite paste electrodes. Platinum foil and Ag|AgCl electrodes acted as counter and reference electrode respectively. Cyclic voltammetry at various scan rates from 0.01 V s^{-1} to 0.3 V s^{-1} was performed at graphite paste modified electrode to analyse the dependency of scan rate (ν) on the peak current density (j). Electrochemical oxidation and reduction of H_2O_2 were performed in 0.1 M phosphate buffer (pH=7.0) containing 0.5 M KCl as supporting electrolyte.

The modified electrode was made through adsorption of PBNPs solution or AuNPs assembled PBNPs solution onto the graphite powder (1-2 μm) and dried at 60 °C overnight. The active paste having composition: (i) PBNPs and AuNPs-PBNPs 2.5% (w/w), graphite powder 67.5% (w/w), nujol oil 30% (w/w). The well of the electrode body (MF-2010) (electrode was obtained from Bioanalytical systems, West Lafayette, IN USA) was filled with active graphite paste and the electrode paste surface was manually smoothed on a clean paper.

1.2.5 Peroxidase like activity of PBNPs and AuNPs assembled PBNPs

Peroxidase like activity of PBNPs and with AuNPs was determined as described earlier [(Pandey and Panday 2016b; Pandey and Pandey 2013d)]. In a typical situation, the peroxidase like activity of as synthesized PBNPs and AuNPs assembled PBNPs was determined spectrophotometrically by measuring the synthesis of oxidised product of o-dianisidine at 430 nm (ε= 11.3 mM^{-1} cm^{-1}) using Hitachi U-2900 spectrophotometer as described earlier [(Pandey and Panday 2016b)]. The measurement was made by formation of oxidized product of o-dianisidine (which is brown in colour) in 0.1 M phosphate buffer (pH=7.0) in the presence of varying concentration of H_2O_2 (0-25 mM) and 50 μM o-dianisidine at 25°C keeping constant concentration of PBNPs.

The steady state kinetics was performed as described earlier [(Pandey and Panday 2016b)]. In a typical situation, steady state kinetics was performed by varying the H_2O_2 concentration (0-25 mM) at fixed concentration of o-dianisidine (50 μM). Each reaction was performed in 2 ml phosphate buffer (0.1 M, pH=7). The variation of absorbance was taken as function of time at fixed wavelength 430 nm (ε= 11.3 mM^{-1} cm^{-1}). Michaelis-Menton equation was used to calculate the kinetic parameters by fitting the absorbance data by the following equation:

$$V = V_{max} [C]/K_m + [C] \qquad (1)$$

Where V represents for rate of conversion, V_{max} is the maximal reaction velocity, C is the concentration of the substrate and K_m is the Michaelis-Menton constant.

1.3 Results

1.3.1 PEI mediated synthesis of nanocrystalline PBNPs and AuNPs assembled PBNPs

Polyethylenimine mediated synthesis of nanocrystalline PBNPs was analyzed by UV-Vis spectroscopy and by simple photoimaging of their respective

solutions. In the first instance, we analyzed the role of each component in this PEI mediated conversion of potassium ferricyanide into PBNPs. Figure.4.1. represents role of each components in this PBNPs synthesis and revealed that all three components are required for the efficient synthesis of PBNPs at 60 °C in 3 hours.

Next phase of study is the optimization of PBNPs synthesis. The optimum concentration of each component was investigated based on the visual photographs and the corresponding UV-Vis spectroscopy while one component was absent and all other components were present in the reaction mixture. Figure 4.2 and Figure.4.3 shows the optimization of PEI mediated synthesis of PBNPs. Figure.4.2. shows the UV-Vis spectra of the system containing constant concentrations of $K_3[Fe(CN)_6]$ (25 mM) and varying concentrations of PEI between 10 mg/ml to 40 mg/ml. Inset to the each figure shows the respective solution photograph (Table.4.1).

Figure.4.3. shows the UV-Vis spectroscopy of the system containing constant concentrations of PEI (20 mg/ml) and varying concentrations of $K_3[Fe(CN)_6]$ (10 mM to 50 mM). Inset to each figure illustrates the visual photograph of the respective solutions (Table.4.2).

1.3.2 Structural characterization

Structural characterization of as synthesized PBNPs and AuNPs assembled PBNPs was done by X-ray diffraction analysis (XRD) and Transmission Electron Microscopy (TEM).

The as synthesized PBNPs and AuNPs assembled PBNPs was characterized by XRD analysis. Figure.4.5. (A) shows the x-ray diffractogram of as synthesized PBNPs and Figure.4.5. (B) for AuNPs assembled PBNPs. In Figure.4.5.(A) shows the characteristic peaks available in the PBNPs (2θ values are 17.4°, 24.7°, 35.3° and 39.6°) and Figure.4.5.(B) represents the characteristic peak of AuNPs (2θ values are 28.2°, 38.3° and 72.2°) along with the characteristic peaks of PBNPs.

To further characterize the same, TEM analysis was performed. Figure.4.6. (A) shows the TEM image of as synthesized PBNPs and Figure.4.6. (B) shows TEM

image of AuNPs assembled PBNPs. This shows that the particles are in the range of 5 nm to 25 nm.

1.3.3 Electrochemical characterization of PEI mediated synthesized PBNPs

The electrochemical behaviour of as synthesized PBNPs was performed to verify the synthesis of PBNPs and the effect of AuNPs on the nanogeometry of PBNPs. Figure.4.7. shows the electrochemical behaviour of PBNPs and AuNPs assembled PBNPs at increasing scan rates between 0.01 V s^{-1} to 0.3 V s^{-1} on graphite paste electrode in 0.1 M KNO_3 as a supporting electrolyte. Figure.4.7.(A) and Figure.4.7.(B) shows the electrochemical behaviour of PBNPs and AuNPs assembled PBNPs respectively. There are two characteristic redox couple presents in the voltammogram of as synthesized PBNPs and AuNPs assembled PBNPs which are at -0.2 V and 0.9 V *vs.* Ag|AgCl. In order to understand the charge transport characteristics within the reaction layer, the cathodic and anodic peak current densities have been plotted against scan rate and square root of scan rate at characteristic peak potential for PBNPs and AuNPs assembled PBNPs as shown in Figure.4.8.

1.3.4 Peroxidase mimetic activity of PBNPs and AuNPs assembled PBNPs

PBNPs and its mixed metal analogues have good stability so this could be a potential mimetic candidate. In previous chapters, we have analyzed the peroxidase mimetic activity of PBNPs synthesized through mediation of THF and H_2O_2. Therefore, it is intended to know the peroxidase mimetic activity of PEI mediated synthesized PBNPs and AuNPs assembled PBNPs. Peroxidase mimetic activity was performed as described in the earlier chapters. Figure.4.9. and Figure.4.10. represents the peroxidase mimetic activity graph for PBNPs and AuNPs assembled PBNPs. Figure.4.9.(B) and Figure.4.10.(B) shows that as synthesized PBNPs and AuNPs assembled PBNPs show Michaelis-Menton equation and the K_m was found to be 2.4 mM and 1.3 mM respectively.

1.3.5 Electrocatalytic reduction and oxidation of H_2O_2 over PBNPs and AuNPs assembled PBNPs modified electrode

1.3.5.1 Cyclic voltammetric and amperometry

The reduction and oxidation of H_2O_2 was performed over PBNPs and AuNPs assembled PBNPs modified graphite paste electrode in 0.1 M phosphate buffer (pH=7.0) containing 0.5 M KCl. The cyclic voltammogram for reduction of H_2O_2 over PBNPs and AuNPs assembled PBNPs modified electrode is shown in Figure. 4.11. It can be seen that the H_2O_2 reduction has increased much in the presence of AuNPs in PBNPs on the addition of an identical concentrations of H_2O_2. Figure.4.12. shows the typical amperometric responses of PBNPs and AuNPs assembled PBNPs system respectively, on the successively additions of H_2O_2 in 0.1 M phosphate buffer containing 0.5 M KCl (pH=7.0). Increase in the reduction current on the successive addition of H_2O_2 over PBNPs modified electrode represents the catalytic property of the modified electrode. Figure.4.13. shows the calibration plots of PBNPs and AuNPs assembled PBNPs respectively. The sensitivity of PBNPs and AuNPs assembled PBNPs modified electrode for H_2O_2 analysis was found to be 34.7 μA mM^{-1} cm^{-2} and 84.9 μA mM^{-1} cm^{-2} with lowest detection limit was 200 nM and 50 nM respectively.

Electrocatalytic oxidation of H_2O_2 over PBNPs and AuNPs assembled PBNPs was studied by cyclic voltammetry and amperometry in 0.1 M phosphate buffer containing 0.5 M KCl (pH=7.0). Figure.4.15. shows the cyclic voltammetry of PBNPs and AuNPs assembled PBNPs. As can be seen from figure, there is an increase in oxidative current beyond 0.5 V *vs.* Ag|AgCl. Figure.4.16. shows the amperometric analysis of electrocatalytic oxidation of H_2O_2 over PBNPs and AuNPs assembled PBNPs modified electrode at 0.6 V *vs.* Ag|AgCl. As can be seen that in case of AuNPs assembled PBNPs have more catalytic current in comparison to PBNPs. Figure.4.17. shows the calibration curve of H_2O_2 oxidation over PBNPs and AuNPs assembled PBNPs. The sensitivity of PBNPs and PBNPs-AuNPs modified electrode for H_2O_2 analysis was found to be 12 μA mM^{-1} cm^{-2} and 56 μA mM^{-1} cm^{-2} with lowest detection limit was 20 μM and 5 μM respectively.

1.3.5.2 Chronoamperometric response

In support of such findings, we investigated the catalytic rate constant (K_{cat}) associated to H_2O_2 sensing over the PBNPs and AuNPs assembled systems. To know the catalytic rate constant (K_{cat}), chronoamperometry was done over PBNPs and AuNPs assembled PBNPs modified graphite paste electrode. Figure.4.14. shows the chronoamperograms for PBNPs (A) and AuNPs assembled PBNPs (B) modified electrodes in absence and in the presence of 1 mM H_2O_2 by setting the step potential at -0.05 V *vs*. Ag|AgCl for subsequent evaluation of I_{cat} and I_L. The plot of I_{cat}/I_L *vs.* $t^{1/2}$ is shown in insets to Figure.4.14.(A') and (B') for PBNPs and AuNPs assembled PBNPs modified graphite paste electrode respectively.

1.3.6 Magnetic measurement of PBNPs and AuNPs assembled PBNPs

Magnetic measurement for PBNPs and AuNPs assembled PBNPs was done to evaluate the magnetic properties of as synthesized PBNPs. Magnetic measurement was performed by the respective powder samples. The variation of magnetization as a function of both temperature and magnetic field were carried out using MPMS vibrating sample magnetometer measurement system. The filed cooled (FC) and zero-field cooled (ZFC) DC magnetization curve were carried out in the temperature range 2 K to 10 K at different external probing magnetic field of 25 Oe, 50 Oe and 100 Oe [Figure.4.18.(A) – (C)]. As can be seen from Figure.4.18. (D) as made PBNPs displays superparamagnetism having high saturation magnetization. Figure.4.19 shows the Normalized zero-field-cooled (ZFC) and field-cooled (FC) magnetizations of PBNPs (A) and AuNPs assembled PBNPs (B) at 100 Oe applied field (H).

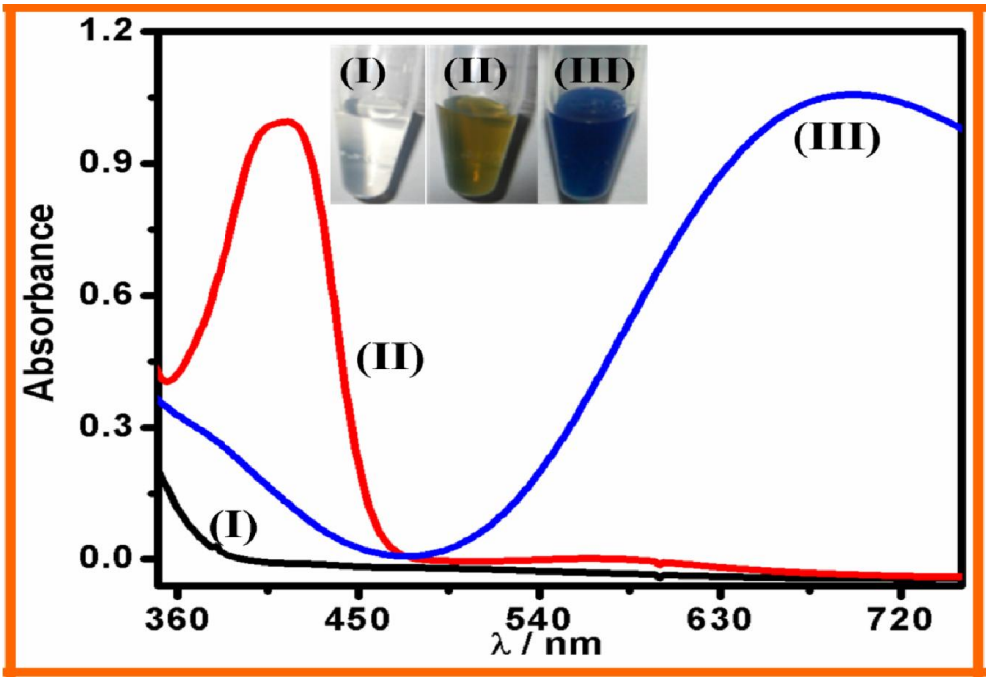

Figure.4.1. UV-Vis spectra of showing requirement of optimum concentration of both $K_3[Fe(CN)_6]$ and PEI in acidic medium for the synthesis of PBNPs.

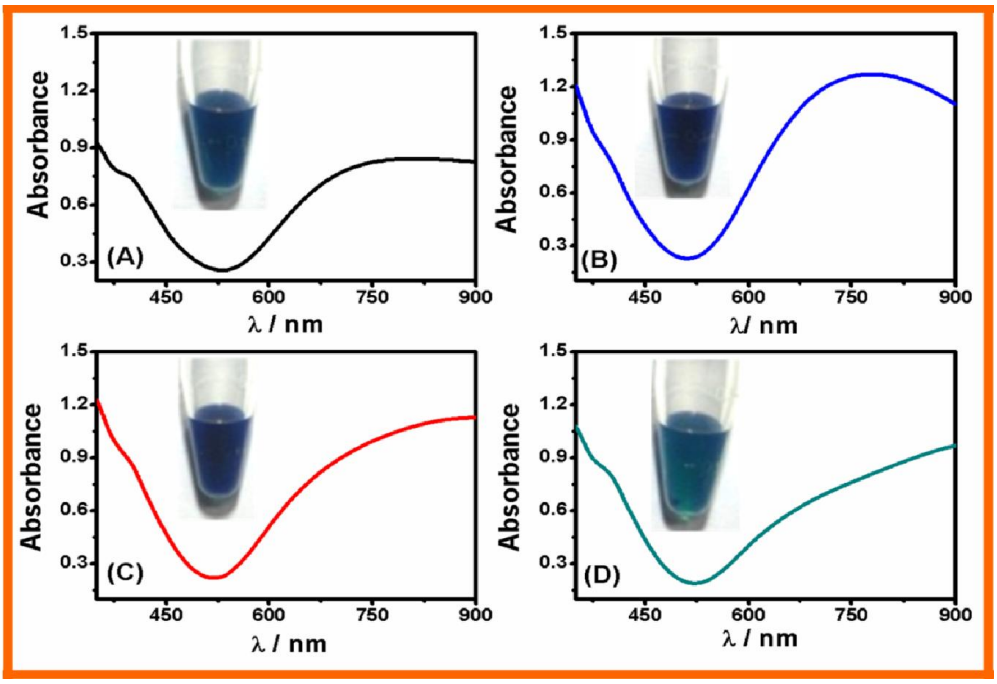

Figure.4.2. UV-Vis spectra of system containing constant concentration of $K_3[Fe(CN)_6]$ (25 mM) and the varying concentration of PEI (A) 10 mg/ml (B) 20 mg/ml) (C) 30 mg/ml and (D) 40 mg/ml.

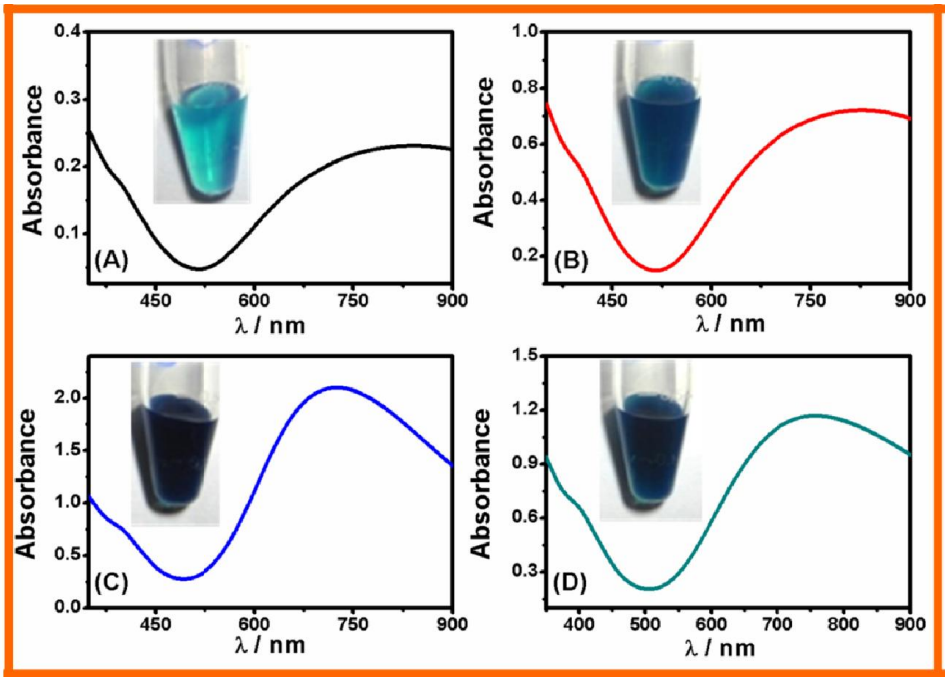

Figure.4. 3. UV-Vis spectra of system containing constant concentration of PEI (20 mg/ml) and the varying concentrations of $K_3[Fe(CN)_6]$ (A) 10 mM (B) 25 mM (C) 35 mM and (D) 50 mM respectively.

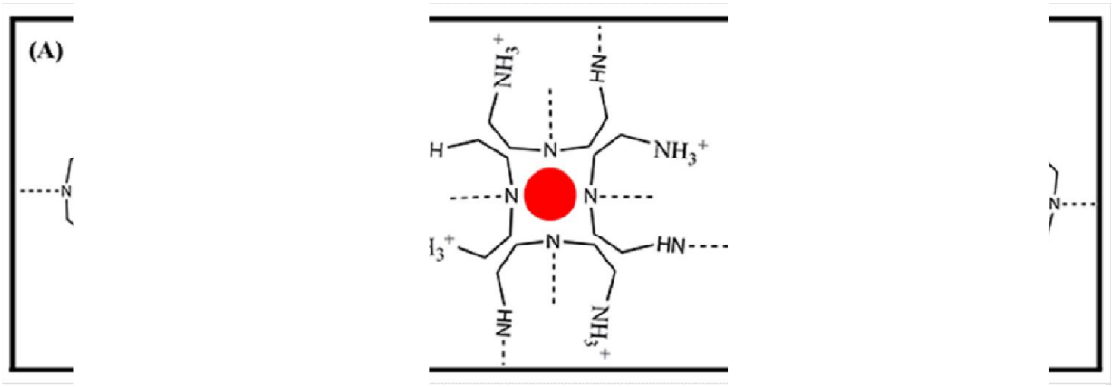

Figure.4. 4. Schematic presentation of cationic polymer coating and formation of PBNPs (A), AuNPs (B) and AuNPs assembled on cationic surface of PBNPs (C).

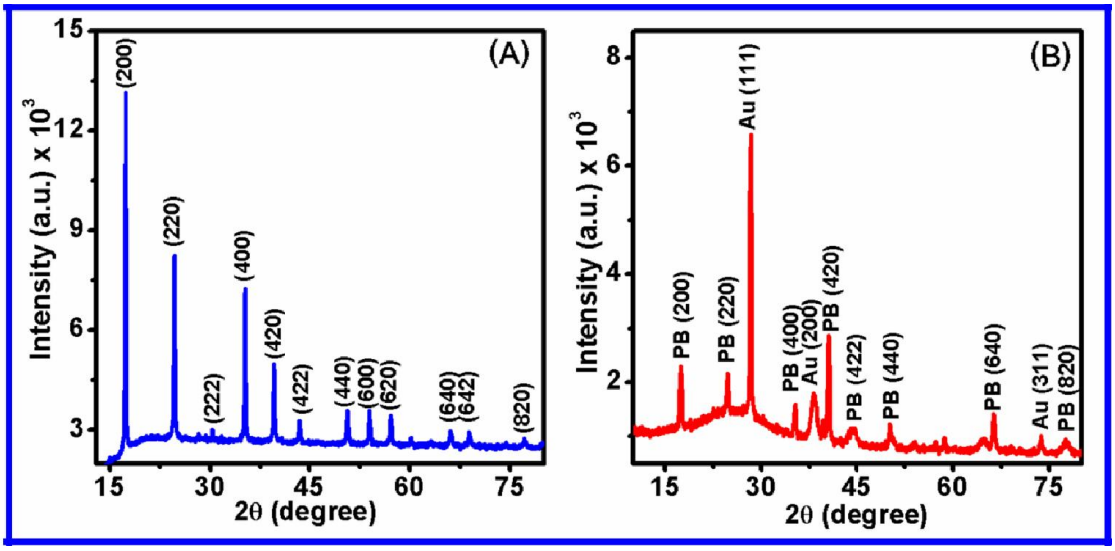

Figure.4. 5. XRD pattern of PBNPs (A) and AuNPs assembled PBNPs (B).

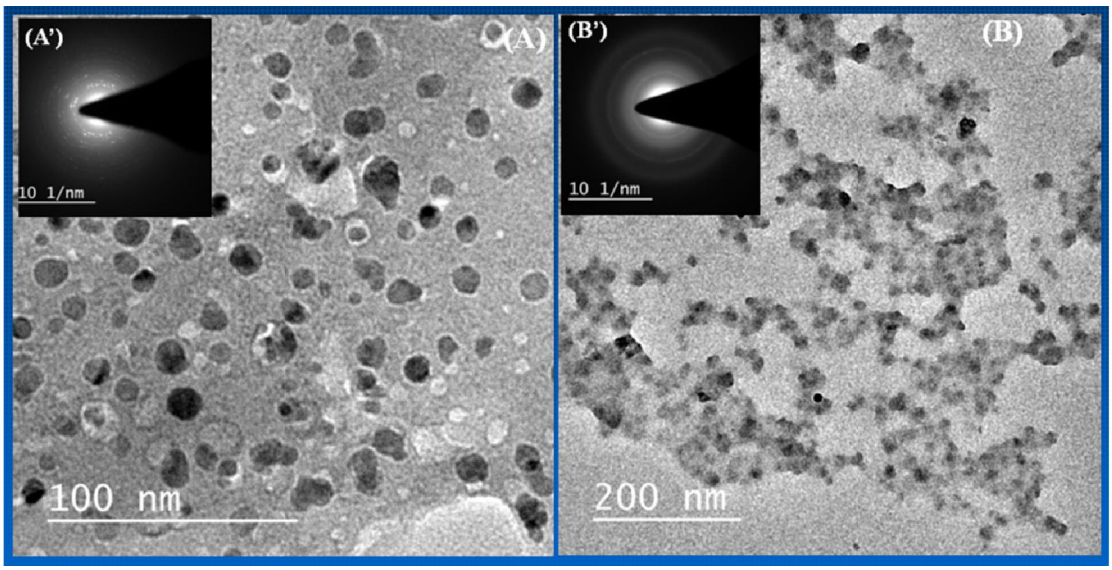

Figure.4. 6. TEM image of PBNPs (A) and AuNPs assembled PBNPs (B). Inset to the figure shows selected area electron diffraction pattern.

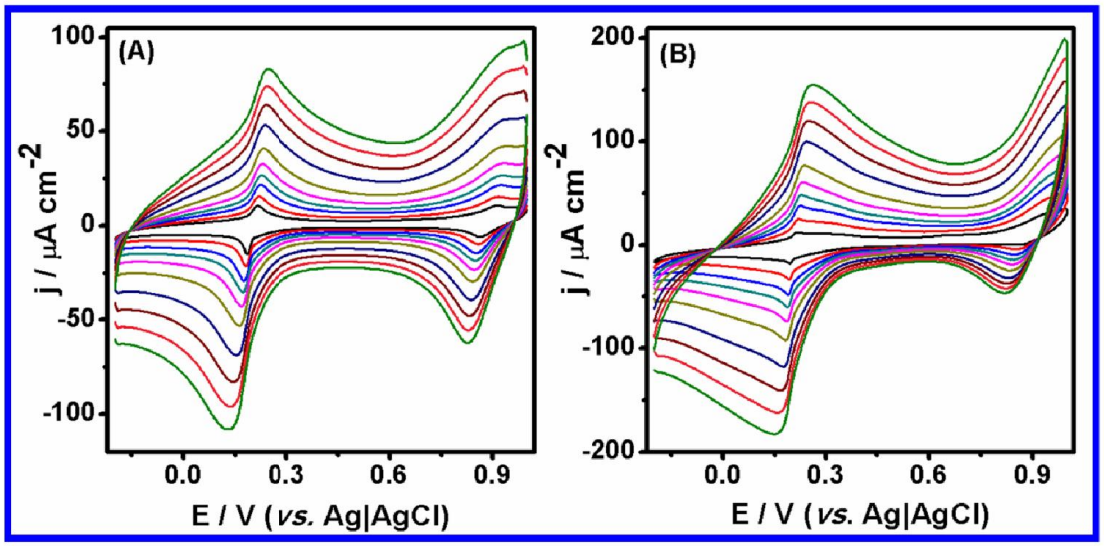

Figure.4. 7. Cyclic voltammograms of PBNPs (A) and AuNPs assembled PBNPs (B) electrode in 0.1 M KNO_3 at the scan rate of: 10, 20, 35, 50, 70, 100, 150, 200, 250, and 300 mV s^{-1} consecutively.

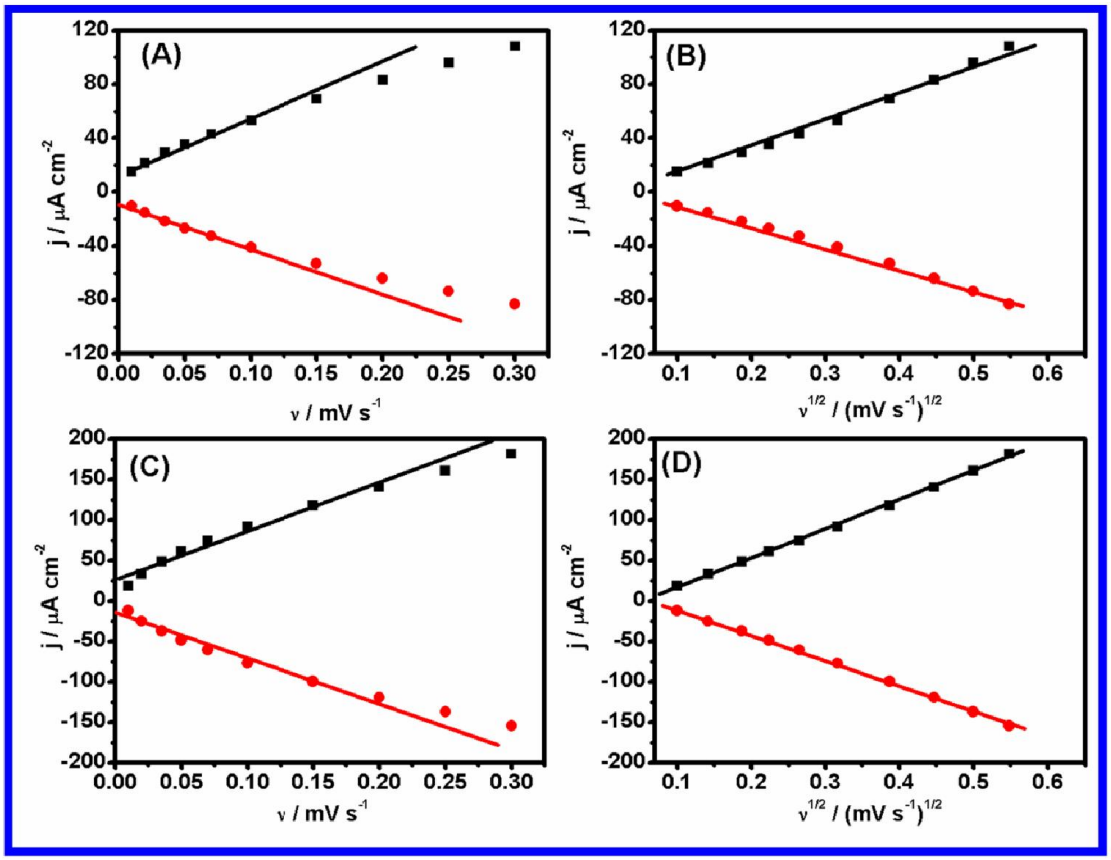

Figure.4. 8. The plot of anodic and cathodic current density *vs.* scan rate (A and C) and square root of scan rate (B and D) for PBNPs (A and C) and AuNPs assembled PBNPs (B and D) respectively.

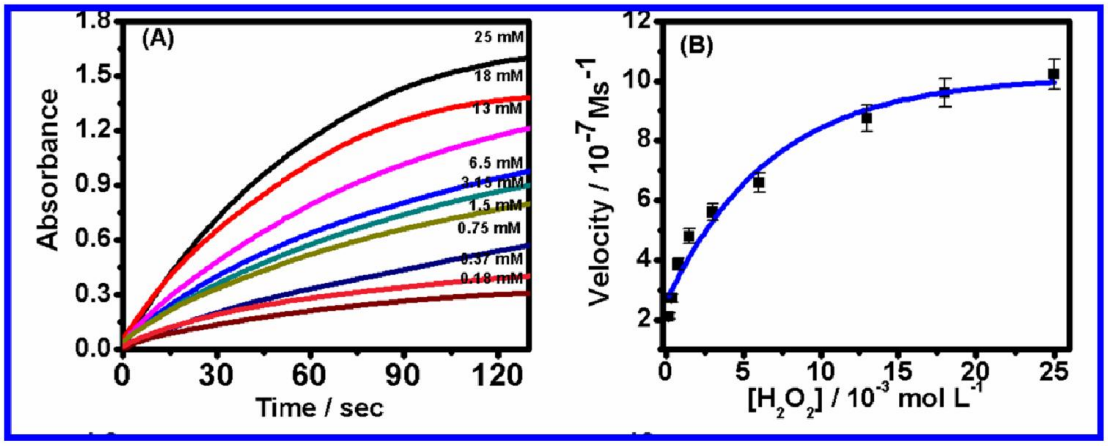

Figure.4.9. Time dependent absorbance changes at 430 nm in the presence of different concentrations of H_2O_2 (from 0.18 mM to 25 mM) and fixed concentration of o-dianisidine (50 µM) catalyzed by PBNPs (A) and Kinetic analysis of PBNPs (B).

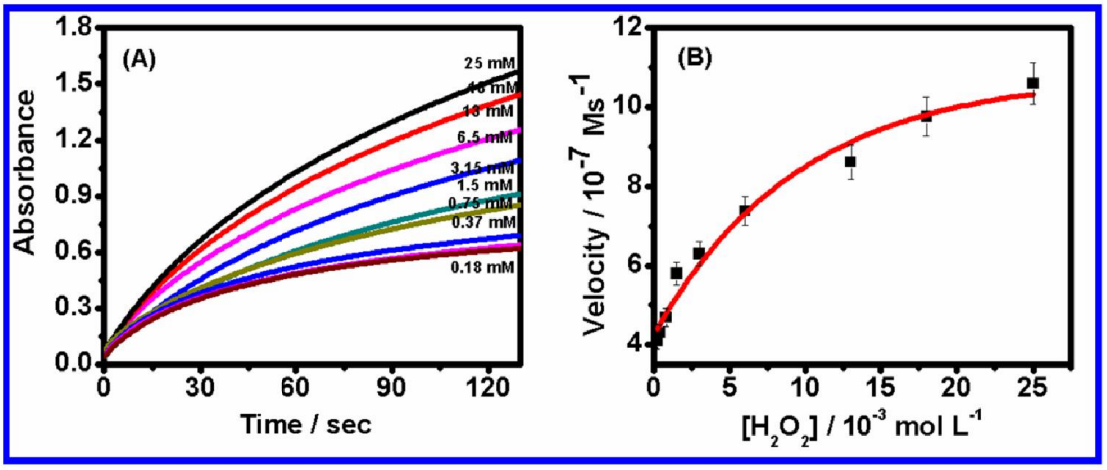

Figure.4.10. Time dependent absorbance changes at 430 nm in the presence of different concentrations of H_2O_2 (from 0.18 mM to 25 mM) and fixed concentration of o-dianisidine (50 µM) catalyzed by AuNPs assembled PBNPs (A), and Kinetic analysis of AuNPs assembled PBNPs (B).

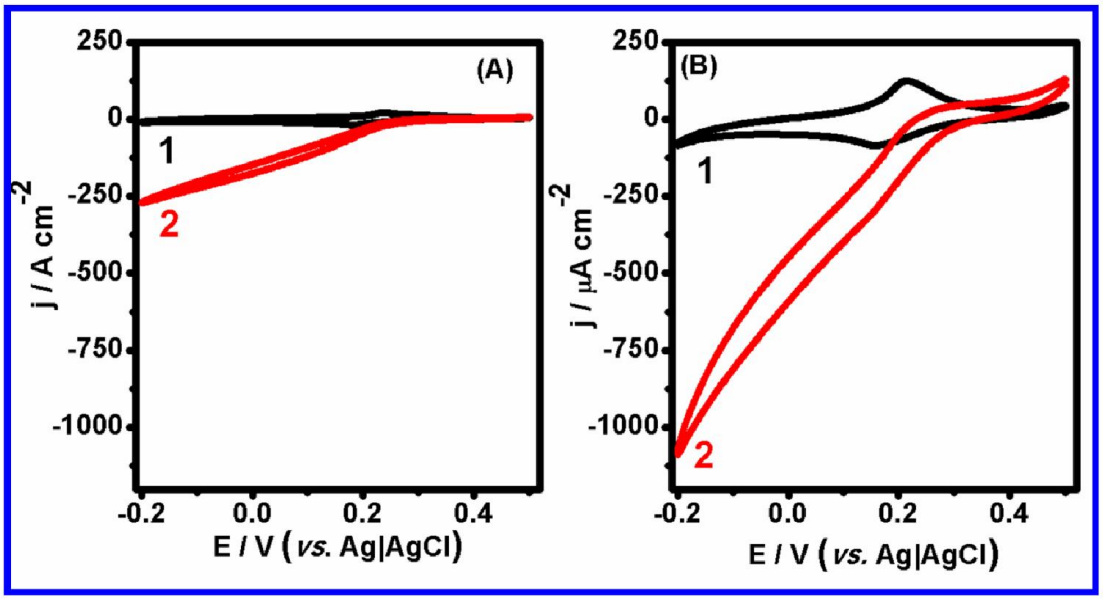

Figure.4.11. Cyclic voltammograms of PBNPs (A) and AuNPs assembled PBNPs (B) in absence (1) and the presence (2) of 1 mM H_2O_2 at the scan rate of 0.01 V s^{-1} in 0.1 M phosphate buffer (pH=7.0) containing 0.5 M KCl.

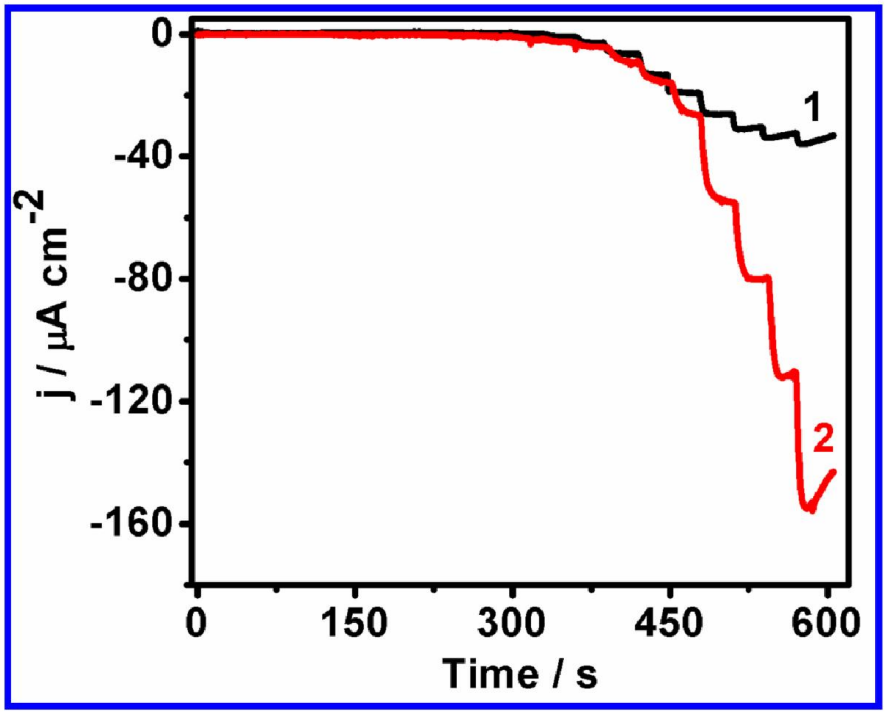

Figure.4.12. Amperometric response of PBNPs (1) and AuNPs assembled PBNPs (2) modified electrodes at 0.2 V *vs.* Ag|AgCl on the addition of varying concentrations of H_2O_2 in 0.1 phosphate buffer containing 0.5 M KCl.

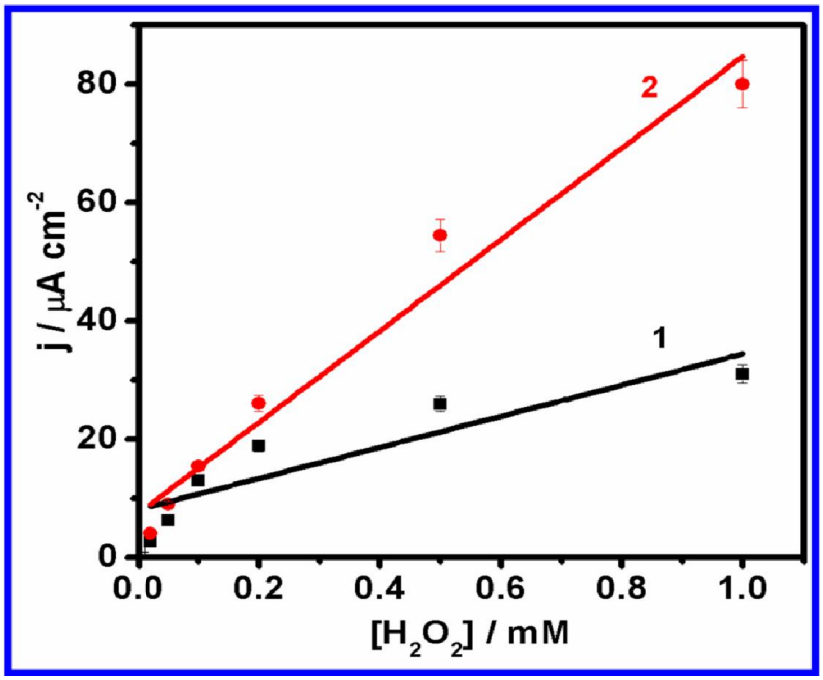

Figure.4.13. Calibration curve of H_2O_2 reduction obtained from amperograms of PBNPs (1) and AuNPs assembled PBNPs (2).

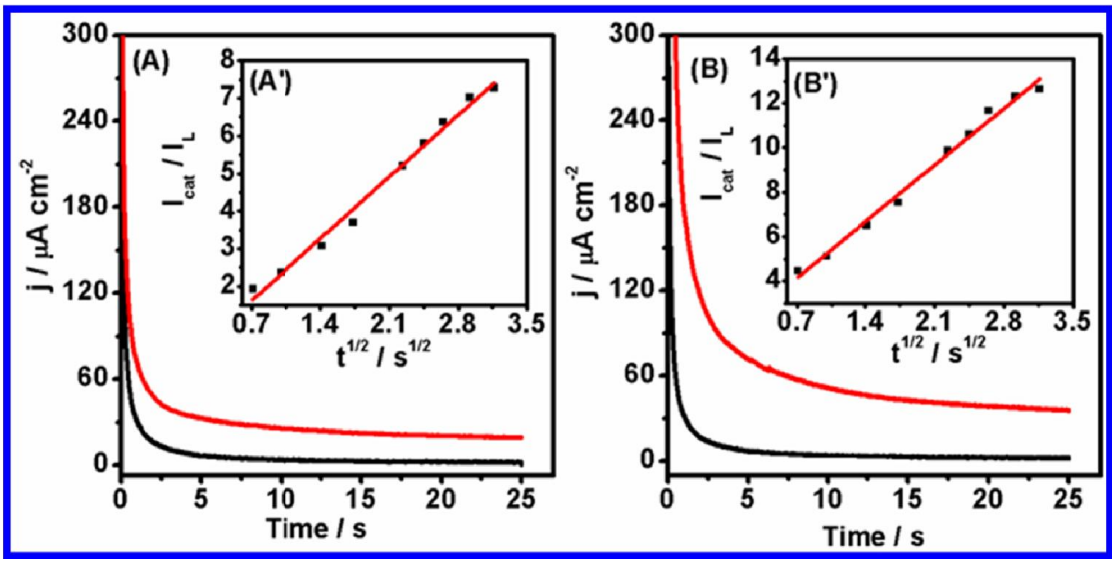

Figure.4.14. Chronoamperograms for PBNPs (A) and AuNPs assembled PBNPs (B) modified electrode in the absence (black curve) and in the presence (red curve) of 1 mM H_2O_2. The step potential was -0.05 V *vs.* Ag|AgCl. Inset: corresponding plots of I_{cat}/I_L vs. $t^{1/2}$ in 0.1 M phosphate buffer containing 0.5 M KCl as supporting electrolyte.

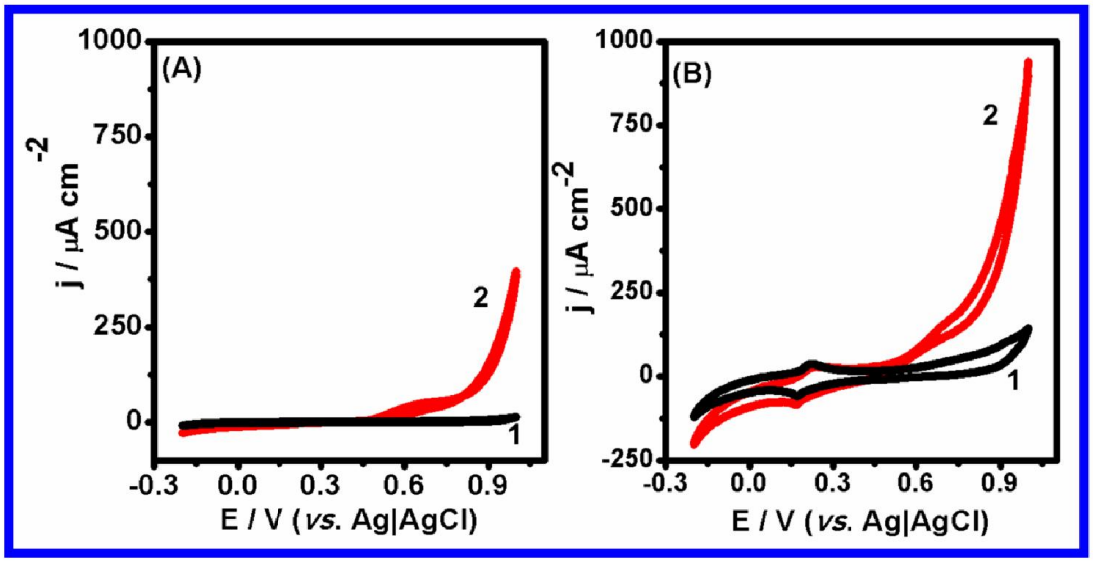

Figure.4.15. Cyclic voltammograms of PBNPs (A) and AuNPs assemble PBNPs (B) in absence (1) and presence (2) of 1 mM H_2O_2 at the scan rate of 0.01 V s^{-1} in 0.1 M phosphate buffer (pH=7.0) containing 0.5 M KCl.

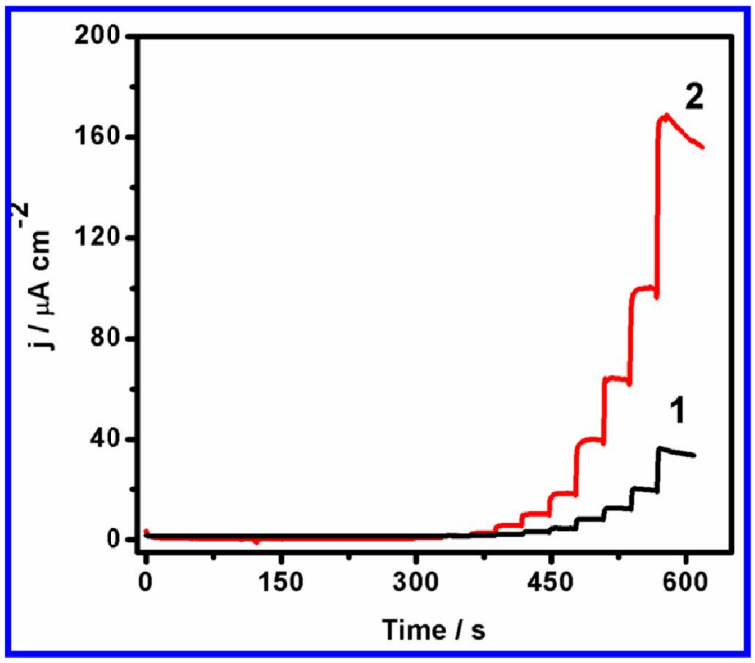

Figure.4.16. Amperometric response of PBNPs (1) and AuNPs-PBNPs (2) modified electrodes at 0.6 V *vs.* Ag|AgCl on the addition of varying concentrations of H_2O_2 in 0.1 phosphate buffer (pH=7.0) containing 0.5 M KCl.

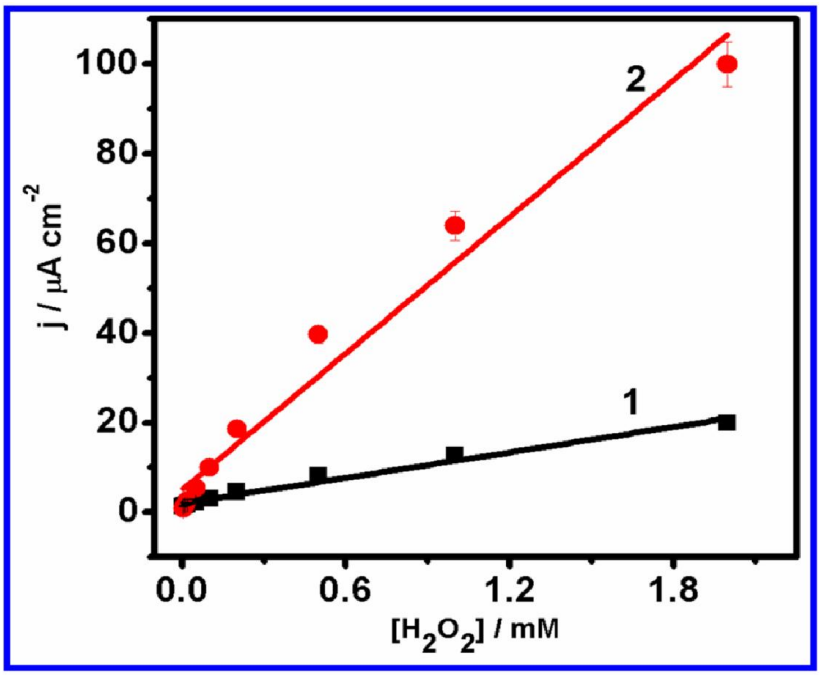

Figure.4. 17. Calibration curve of oxidation of H_2O_2 obtained from amperograms of PBNPs (1) and AuNPs assembled PBNPs (2).

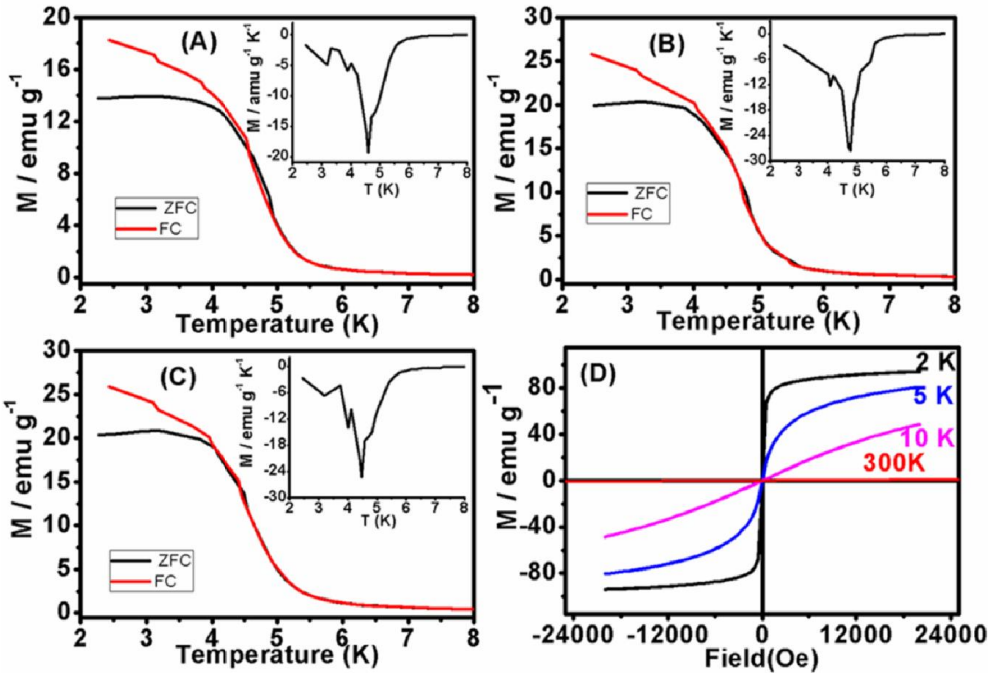

Figure.4.18. Normalized zero-field-cooled (ZFC) and field-cooled (FC) magnetizations of PBNPs at different applied field (H): A=25, B=50 and C=100 Oe; (D) Magnetization hysteresis loops at 2 K, 5 K, and 10 K respectively (D).

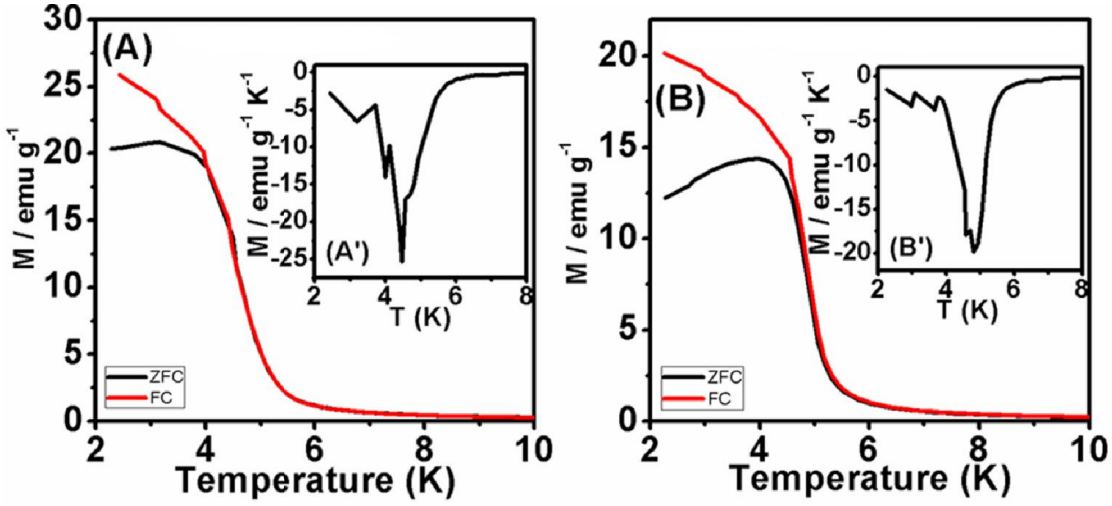

Figure.4.19. Normalized zero-field-cooled (ZFC) and field-cooled (FC) magnetizations of PBNPs (A) and AuNPs assembled PBNPs (B) at 100 Oe applied field (H).

1.4 Discussion

1.4.1 PEI mediated synthesis of nanocrystalline PBNPs

At first instant, attempts were made to understand the process of PEI mediated conversion of $K_3[Fe(CN)_6]$ into PBNPs. The results demonstrate that PEI enabled the conversion of $K_3[Fe(CN)_6]$ into PBNPs at 60 ^oC within 3 hours. The results as shown in Figure.4.1. demonstrates the role of each component $K_3[Fe(CN)_6]$ and PEI during proposed reaction protocol for PBNPs synthesis. The composition of each reacting components *i.e.* $K_3[Fe(CN)_6]$ and PEI, play important role during such conversion. The findings as shown in Figure.4.1. justified that when all the components are present in optimum concentration, only allowed the conversion of single precursors into stable, well dispersed, polycrystalline PBNPs at 60 °C in 3 hours as shown in Figure.4.1.(III). In absence of either components does not lead to the synthesis of PBNPs as shown in [Figure.4.1.(I) and (II)] respectively.

Figure.4.2 and Figure.4.3. shows the optimum concentrations of $K_3[Fe(CN)_6]$ and PEI, required for such conversion having better PB character as evaluated from the absorbance recorded at 680 nm, was achieved by varying the concentration of one

component while keeping fixed concentration of other component and *vice versa*. The composition of each component play important role in such conversion as shown in Table.4.1 and Table.4.2.

PEI in acidic medium precisely controls the nucleation of PBNPs from $K_3[Fe(CN)_6]$ followed by conversion of the same into positively charged polymer as shown in Figure.4.4. (A). The negatively charged centres of Prussian blue (PB) facilitate electrostatic interaction with cationic polymer centre leading to cationic polymer coating blocking a specific number of coordination sites on the transition metal ions, thereby preventing the formation of infinite structures and facilitating the probability of nanoparticle formation. Under similar condition, the exchange of $K_3[Fe(CN)_6]$ with gold salt ($HAuCl_4$) yield into the formation of AuNPs as shown in Figure.4.4. (B). When the formation of AuNPs is allowed to take place in the solution containing as made PBNPs, the self assembly of AuNPs on polycationic surface is observed as shown in Figure.4.4. (C) displaying several fold enhancement in catalytic behaviour of material.

1.4.2 Characterization of cationic polymer coated PBNPs and AuNPs assembled PBNPs

Characterization was performed by X-ray diffraction (XRD) analysis and Transmission Electron Microscopy (TEM) analysis.

1.4.2.1 XRD analysis of PBNPs and AuNPs assembled PBNPs

X-ray diffraction analysis was performed by the PBNPs and AuNPs assembled PBNPs powder which was obtained by drying the respective solutions at 60 °C overnight.

X-ray diffractogram of PBNPs and AuNPs assembled PBNPs is shown in Figure.4.5. X-ray diffractogram of as synthesized PBNPs is shown in Figure.4.5. (A). Figure.4.5. (A) shows peaks at c.a. 17.4° (200), 24.7° (220), 35.3° (400), 39.6° (420), and 43.7° (422), 50.0° (440), 53.9° (600), 57.2° (620), 66.1° (640), 68.9° (642) and 77.2° (820) which can be indexed as the PB cubic space group *Fm3m* [(Ding *et al.* 2009; Lee 2003; Samain *et al.*

2013)]. The crystallite size of as synthesize was found to be 42.3 nm, 39.2 nm, 47.9 nm, 38.5 nm and 48.7 nm on the peak at 17.4°, 24.7°, 35.2°, 39.5° and 43.0° (2θ values).

X-ray diffractogram of as synthesized AuNPs assembled PBNPs is shown in Figure.4.5. (B). This figure contains peaks at c.a. 28.2°, 38.3°, and 74.2° (2θ value) which can be assigned as (111), (200) and (311) respectively corresponding to the face-centered cubic (fcc) phase of gold. Along with these peaks, there are few other peaks in AuNPs assembled PBNPs at c.a. 17.6°, 24.8°, 35.5°, 44.3°, 50.4°, 66.1° and 66.1° (2θ value) which can be assigned to (200), (220), (400), (422), (440), 640) and (820) for PB phases.

1.4.2.2 TEM analysis of PBNPs and AuNPs assembled PBNPs

The particle size and morphology of as synthesize PBNPs and AuNPs assembled PBNPs were characterized by Transmission Electron Microscopy (TEM). Figure.4.6. represents the TEM analysis of both PBNPs and AuNPs assembled PBNPs. TEM analysis was performed by drop casting the respective samples on the carbon coated copper grid and dried at room temperature.

Figure.4.6. (A) represents the TEM image of as synthesized PBNPs and the inset to this Figure.4.6. (A') shows the respective selected area electron diffraction pattern (SAED) of as synthesized PBNPs justifying excellent polycrystalline behaviour.

Figure.4.6. (B) represents TEM image of AuNPs assembled PBNPs and inset to this figure [Figure.4.6.(B')] shows the SAED pattern of the same. TEM image and diffraction pattern confirms the formation of AuNPs assembled PBNPs.

1.4.3 Electrochemistry and catalytic activity of PBNPs and AuNPs assembled PBNPs modified electrode

Cyclic voltammograms of as synthesized PBNPs is shown in Figure.4.7. (A). Water soluble PBNPs display excellent redox

electrochemistry. Two reversible redox couples are observed between potential ranges of -0.2 to 1.0 V *vs*. Ag|AgCl displaying first redox peaks corresponding to the oxidation of Prussian white and reduction of Prussian blue along with second redox couple at 0.9 V for the oxidation of Prussian blue and reduction of Berlin green [(Ricci and Palleschi 2005)].

Figure.4.7. (B) represents the cyclic voltammograms of as synthesized AuNPs assembled PBNPs. The self assembly of AuNPs facilitate both relatively faster oxidation and reduction processes with significant increase in cathodic and anodic current under similar condition as shown in Figure.4.7. (B).

An analysis of the electrochemical behaviour of PBNPs and AuNPs assembled PBNPs was performed from the plot of peak current density (j) *vs.* scan rate (ν) of the PB/PW redox couples in the range of -0.2 V to 0.5 V *vs*. Ag|AgCl. Figure.4.8. (A) and (B) shows the plot of peak current density (j) *vs.* scan rate (ν) and the plot of peak current density (j) *vs.* square root of scan rate ($\nu^{1/2}$) for PBNPs. Similarly, Figure.4.8. (C) and (D) shows the plot of peak current density (j) *vs.* scan rate (ν) and the plot of peak current density (j) *vs.* square root of scan rate ($\nu^{1/2}$) for AuNPs assembled PBNPs. The result shown in Figure.4.8. (A) and (C) justified that peak current density (j) tends to be linear with the increase in scan rate (ν) up to 0.15 V s^{-1} and 0.2 V s^{-1} in case of PBNPs and AuNPs assembled PBNPs systems respectively, indicating charge transport from a surface-confined redox species. At higher scan rates, j was found to vary linearly with the square root of the scan rate ($\nu^{1/2}$) as shown in Figure.4.8.(B) and (D) indicating a change in the reaction kinetics to a diffusion-limited process.

1.4.4 Homogeneous catalysis of PBNPs and AuNPs assembled PBNPs

Figure.4.9. (A) represents the time dependent absorbance changes at 430 nm in the presence of different concentrations of H_2O_2 and fixed concentrations of o-dianisidine for PBNPs sol. Figure.4.9. (B) shows the Michaelis-Menton saturation curve and justified that as synthesized PBNPs

follows the Michaelis-Menton equation. Time dependent absorbance changes at 430 nm in the presence of different concentrations (0.18 mM to 25 mM) of H_2O_2 and fixed concentration of o-dianisidine (50 μM) is recorded with K_m to the order of 2.4 mM for as synthesized PBNPs.

Figure.4.10. (A) represents the time dependent absorbance changes at 430 nm in the presence of different concentrations of H_2O_2 (0.18 mM to 25 mM) and fixed concentrations of o-dianisidine (50 mM) for AuNPs assembled PBNPs. Figure.4.10. (B) justified that the as synthesized AuNPs assembled PBNPs follows Michaelis-Menton equation. Cooperative self assembly of AuNPs significantly improve the K_m value to the order of 1.3 mM and compared to those with horseradish peroxidase under normalized conditions of catalyst concentrations to the order of 3.68 mM. Such an impressive K_m for as made material manifests its significance as perfect peroxidase replacement in biomedical application.

1.4.5 PBNPs and AuNPs assembled PBNPs mediated reduction of H_2O_2

Earlier findings demonstrated that H_2O_2 undergo both direct, electrocatalytic and HRP-mediated reduction at lower potential [(Pandey *et al.* 2003; Pandey *et al.* 2001; Pandey *et al.* 1997)]. In order to resolve the variation in catalytic ability of PBNPs and AuNPs assembled PBNPs, cyclic voltammograms of the respective material modified graphite paste electrodes were examined in absence (1) and presence (2) of 1 mM H_2O_2. Figure.4.11. shows the cyclic voltammetry performed on graphite paste electrode in the absence (1) and presence (2) of 1 mM H_2O_2 for as synthesized PBNPs [Figure.4.11. (A)] and AuNPs assembled PBNPs [Figure.4.11. (B)]. It indicates the significant effect of AuNPs assembled PBNPs compared to PBNPs.

Electrocatalytic reduction of H_2O_2 over as synthesized electrode was done by amperometric analysis at 0.2 V *vs.* Ag|AgCl for PBNPs and self assembled AuNPs on PBNPs which is shown in Figure.4.12. Amperometric measurement was performed under stirring condition in 0.1 M phosphate

buffer containing 0.5 M KCl (pH=7.0). The catalytic activity is again significantly improved after AuNPs assembly as shown from amperograms Figure.4.12. (1) and (2) respectively. The sensitivity of PBNPs and AuNPs assembled PBNPs modified electrode for H_2O_2 analysis was found to be 34.7 μA mM^{-1} cm^{-2} and 84.9 μA mM^{-1} cm^{-2} with lowest detection limit was 200 nM and 50 nM respectively [Figure.4.13]. These findings justified the role of AuNPs assembled PBNPs on the electrocatalytic reduction of H_2O_2 and revealed that nanostructured AuNPs significantly enhances the dynamics of H_2O_2 reduction. Analogous findings similar to that recorded on homogeneous catalysis justifying the usability of as made materials for both homogeneous and heterogeneous systems. Catalytic rate constant (K_{cat}) for PBNPs and AuNPs assembled PBNPs mediated reduction of H_2O_2 has also been investigated as described earlier [(Pandey and Pandey 2012a)] using Cottrell equation as shown below;

$$I_{cat} / I_L = (K_{cat}\, Ct)^{1/2}$$

Where I_{cat} and I_L are the currents of the PBNPs modified electrodes in the presence and absence of H_2O_2 respectively. K_{cat} was calculated from the slope of the I_{cat} / I_L vs. $t^{1/2}$ plot. Figure.4.14. (A) and (B) shows the Chronoamperograms of the system PBNPs and AuNPs assembled PBNPs respectively in the presence and absence of 1 mM H_2O_2. The values for K_{cat} were calculated to be 2.42 x 10^2 $M^{-1}s^{-1}$ and 5.78 x 10^2 $M^{-1}s^{-1}$ for PBNPs and AuNPs assembled PBNPs respectively and justify the significance of as made materials in electroanalytical chemistry [(Pandey and Pandey 2012a)].

1.4.6 PBNPs and AuNPs assembled PBNPs mediated oxidation of H_2O_2

Electrocatalytic oxidation of H_2O_2 has also been studied at the surface of modified electrode. H_2O_2 undergo oxidation at relatively higher potential [(Li *et al.* 2005)]. The PB system reported so far catalyzes the oxidation of H_2O_2 at higher potential i.e. 0.9 V *vs.* Ag|AgCl with reasonable low sensitivity [(Jaffari and Pickup 1996b; Karyakin *et al.* 1995)]. Subsequently, we attempted to understand the electrocatalytic oxidation of H_2O_2 at relatively low potential i.e., 0.6 V *vs.*

Ag|AgCl on the PBNPs or AuNPs assembled PBNPs modified graphite paste electrode. Figure.4.15. shows the electrocatalytic oxidation of H_2O_2 at 0.6 V vs. Ag|AgCl.

Figure.5.15. shows the electrocatalytic oxidation of H_2O_2 at 0.6 V *vs*. Ag|AgCl in carbon paste electrode in 0.1 M phosphate buffer (pH=7.0) containing 0.5 M KCl as supporting electrolyte. Figure.4.15. (A) represents the cyclic voltammograms of as synthesized PBNPs in the absence (1) and presence (2) of H_2O_2 and Figure.4.15 (B) represents the same graph for AuNPs assembled PBNPs. We found that there is significant enhancement for H_2O_2 oxidation in case of AuNPs assembled PBNPs in comparison to PBNPs. Electrocatalytic oxidation of H_2O_2 was quantified by performing the amperometric analysis in 0.1 M phosphate buffer (pH=7.0) containing 0.5 M KCl in continuous stirring mode for PBNPs and AuNPs modified PBNPs. We found that as made material efficiently catalyzed the oxidation of H_2O_2 at 0.6 V *vs.* Ag|AgCl as shown in Figure.4.16. for sensitive electroanalytical sensing of H_2O_2.The sensitivity of PBNPs and AuNPs assembled PBNPs modified electrode for H_2O_2 analysis was found to be 12 μA mM^{-1} cm^{-2} and 56 μA mM^{-1} cm^{-2} with lowest detection limit was 20 μM and 5 μM respectively [Figure.4.17]. The co-operative self assembly of AuNPs further enhance the catalytic activity increasing the sensitivity of sensing based anodic current measurement [Figure.4.16].

1.4.7 Magnetic properties of cationic polymer coated PBNPs and AuNPs assembled PBNPs

The variation of magnetization as a function of both temperature and magnetic field were carried out using MPMS vibrating sample magnetometer measurement system. The filed cooled (FC) and zero-field cooled (ZFC) DC magnetization curve were carried out in the temperature range 2 K to 10 K at different external probing magnetic field of 25 Oe, 50 Oe and 100 Oe. In the FC protocol, the data were collected while the samples were cooled down under the external field whereas in the ZFC protocol, the data were collected in absence of any external magnetic field. As made PBNPs displays superparamagnetism having high saturation magnetization and zero coercivity and remanence as shown

in Figure.4.18. Figure.4.18. (A), Figure.4.18. (B) and Figure.4.18. (C) show the M(T) for zero-field-cooling (ZFC) and filed-cooling (FC) program at different field strength i.e. 25, 50 and 100 Oe with blocking temperature 4.3 K, 4.4 K and 4.2 K for superparamagnetic material.

The magnetic hysteresis loop shown in the Figure.4.18. (D) was measured at different temperature from +2 T to -2 T magnetic field. From the figure significant changes in the magnetic properties of the samples under investigation has been seen. The magnetization of the samples follows the linear relationship at room temperature (i.e., at 300 K) within the measured magnetic field. In contrast to 300 K, the system shows colossal saturation magnetization well below cryogenic temperature i.e., below 5 K. The appearance of non-linearity upon decreasing temperature indicating the presence of super-paramagnetism behaviour in the system. Magnetization hysteresis loops at 2 K, 5 K and 10 K is shown in Figure.4.18.(D) justifying superparamagnetism and manifest for many biomedical and other applications particularly magnetic resonance imaging, drug delivery, hyperthermia, magnetofaction and tunable viscosity [(Lawaczeck *et al.* 2004; Patra *et al.* 2015; Weinstein *et al.* 2010)]. The total magnetic moment of the PBNPs can be regarded as one giant magnetic moment, composed of all the individual magnetic moments. Cooperative self assembly of AuNPs on PBNPs although show superparamagnetic behaviour however, the magnetization saturation is reduced [Figure.4.19. (B)] under similar condition in absence of AuNPs [Figure.4.19. (A)].